Impact of the experimental bandwidth on circularly polarized luminescence measurements of lanthanide complexes: the case of erbium(III).

Annika Sickinger,[a] Bruno Baguenard,[b] Amina Bensalah-Ledoux,[b] Yannick Guyot,[b] Laure Guy,[a] Fabrice Pointillart,[c] Olivier Cador,[c] Maxime Grasser,[c] Boris Le Guennic,[c] François Riobé,[d] Olivier Maury[a,*] and Stéphan Guy[b*]

a. *Univ. Lyon, ENS de Lyon, CNRS Laboratoire de Chimie UMR 5182, Université Claude Bernard Lyon 1, F-69342 Lyon, France.*

b. *Univ. Lyon, Institut Lumière Matière, UMR 5306 CNRS, Université Claude Bernard, Lyon 1, F-69622 Villeurbanne, France.*

c. *Univ Rennes, CNRS, Institut des Sciences Chimiques de Rennes, UMR 6226, F-35000 Rennes, France.*

d. *Institut de Chimie de la Matière Condensée de Bordeaux, CNRS, UMR 5026, F-33608 Pessac, France.*

This article outlines the synthesis and comprehensive characterization of a pair of Er(III) enantiomers with controlled helicity. These complexes exhibit a near-infrared circularly polarized luminescence (NIR-CPL) signature with high g_{lum} values of ± 0.66 at 1519 nm at room temperature. However, due to a large number of potential transitions at this temperature owed to the crystal field splitting, the CPL pattern likely results from overlapping of many positive and negative contributions. This study explores how reducing the effective bandwidth affects the CPL spectral analysis. Practical insights are provided for measuring CPL spectra, highlighting the importance of resolving peak positions with opposite signs to accurately determine g_{lum} values.

Introduction

The synthesis of chiral lanthanide complexes is currently attracting a great deal of interest for the determination of their chiroptical properties such as electronic circular dichroism (ECD) and circularly polarized luminescence (CPL). This interest is particularly focused in the near infrared (NIR) region. In the early 2000s, Parker, Riehl and Di Bari et al. [1-3] were among the pioneers in this field, describing the first ECD properties of ytterbium and neodymium complexes. However, the study of NIR-chiroptical properties was largely ignored for about two decades until recently when NIR-CPL and NIR-ECD spectrometers became commercially available. Since 2019, there has been a significant increase of publications in this field, which has been summarized recently in a review article.[4] Some noteworthy contributions include the work of Zinna and Di Bari,[5-7] Ung,[8] Piccinelli,[9, 10] Pointillart,[11-13] and our group,[14] who have mainly focused on Yb(III) and Sm(III) complexes. Very recently, the NIR-CPL detection was extended to the wavelength range of Er(III) complexes around 1550 nm.[8, 15-18] It is important to note that measuring NIR-luminescence and especially NIR-CPL of lanthanide complexes remains a technical challenge even using the latest advancements in CPL spectrometers equipped with highly sensitive InGaAs detectors (PEM or CCD camera). This is mainly owed to the typically low quantum yields of lanthanide NIR-emitters. The acquisition of luminescence spectra with a satisfying signal-to-noise ratio (S/N) hence requires compromising on either long accumulation (high integration time or collection of several scans) or a higher experimental bandwidth (EBW) increasing the slits aperture for detection, which may decrease the resolution. In this article, we present the synthesis, crystal structure and comprehensive photophysical and chiroptical characterization of a chiral helicoidal Er(III) complex (Fig. 1) based on the previously described functionalized *R,R* (or *S,S*) pyridyldiamide ligands.[14, 19] Additionally, we have used these complexes to demonstrate experimentally and by numerical simulation the crucial impact of EBW on the resolution of the CPL signal and the consistency of corresponding dissymmetry factors.

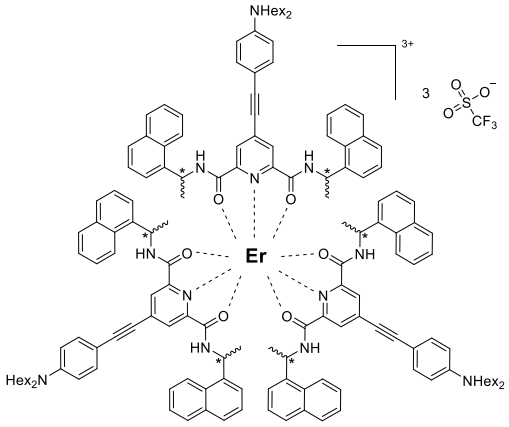

Fig 1. Structure of the chiral Erbium(III) complexes.

Results and Discussion

The chiral Er(III) complex was prepared in the same way as its Yb(III) analogue, which involved the self-assembly of three chiral *R,R* (or *S,S*) pyridyldiamide ligands (for ligand synthesis and characterization cf. SI chapter S3) around the central lanthanide ion.[14] The chirality of the ligand determined the Δ- and Λ-helicity of the resulting complexes [Er(*S,S*-L)$_3$](OTf)$_3$ and [Er(*R,R*-L)$_3$](OTf)$_3$ referred to as **Δ-Er** and **Λ-Er**, respectively. The complexes were fully characterized by NMR and FTIR spectroscopies and mass spectrometry (SI, Scheme S2 and Figures S6-S10).

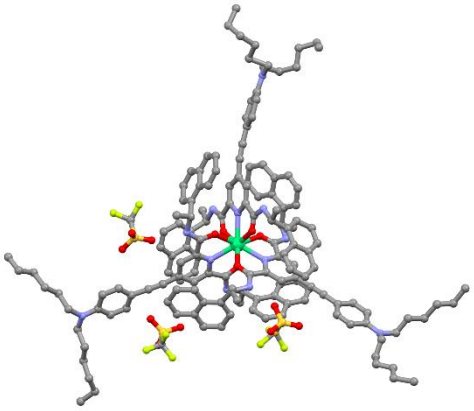

Fig 2. Molecular structure obtained by X-ray diffraction of [Er(*R,R*-L)$_3$](OTf)$_3$·4(MeOH) single crystal (**Λ-Er**). Hydrogen atoms and MeOH solvent molecules of crystallization are omitted for clarity. Green, Er; red, O; blue, N; grey, C; light green, F; yellow, S.

Single orange crystals were obtained through the diffusion of di-*n*-butylether over a concentrated solution of the complex in methanol (Fig 2). The crystal structure of **Λ-Er** was determined using single crystal X-ray diffraction, revealing that it crystallizes in the chiral $P2_12_12_1$ orthorhombic space group (Figure S11 and Table S1). The asymmetric unit consists of one [Er(*R,R*-L)$_3$]$^{3+}$ complex, three TfO^- anions and four methanol solvent molecules. The Er(III) center is coordinated to three tridentate *R,R*-ligands resulting a N3O6 environment and confirming the Λ-type Er(III) centered chirality. The average Er-N bond length (2.46 Å) is longer than the Er-O bond length (2.34 Å) in agreement with the oxophilic nature of the lanthanide. To maintain electro-neutrality, three triflate anions are present: two of them are involved in hydrogen bonds with the amine of the *R,R*-ligand while the third one interacts with one methanol molecule. As for the Yb(III) counterpart, intramolecular π-π interactions are observed between each pyridyldiamide moiety and naphtyl group. The crystal packing indicates that no significant π stacking can take place because of the bulky hexyl chains (Figure S12). A remarkable long shortest intermolecular Er···Er distance of 15.08 Å was found.

The photophysical studies were conducted in diluted methanol solution and all relevant data are summarized in Table 1. The complex solutions exhibit intense orange color and display a broad intense absorption band centered around 455 nm (Figure 3, top, Table S2). This absorption band is assigned to the intra-ligand charge transfer (ILCT) transition from the dialkylamino donor group to the central pyridine bis-amide ligand acting as acceptor. Notably, this transition is significantly red-shifted compared to that of the free ligand (λ_{abs} = 395 nm, $\Delta\lambda$ = 60 nm, Fig. 3) due to the Lewis acidity of the erbium trication.[20, 21] Interestingly, even upon diluting the complex solution to a concentration as low as 4.5 10^{-7} M (Figure S13), no distinct absorption band corresponding to the free ligand appeared, suggesting the absence of potential dissociation processes in the methanol solution.

Fig 3. (Top) Room temperature normalized absorption of the ligand *R,R*-L (dashed line)

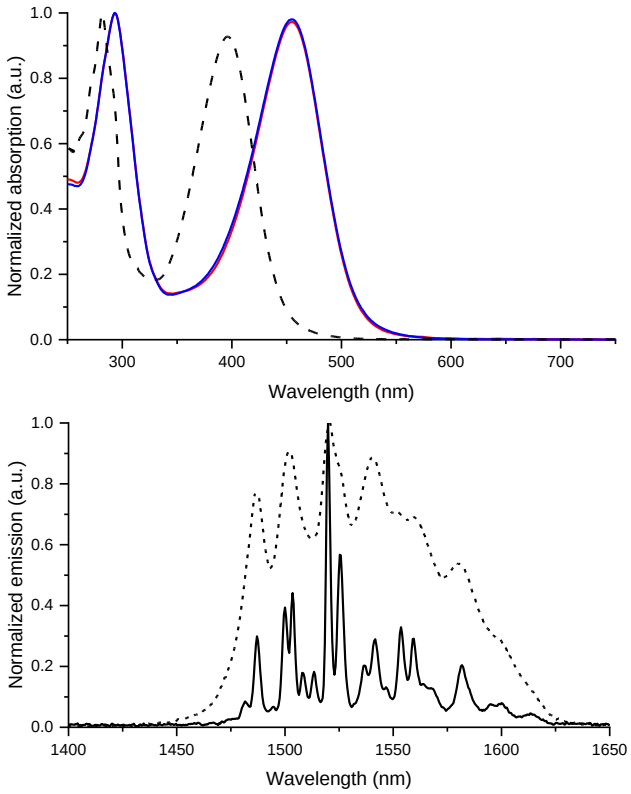

and of **Δ-Er** (blue) and **Λ-Er** (red). (Bottom) Representative normalized luminescence spectra of Λ-Er at room temperature (dashed line) and 77 K (solid line) in MeOH/EtOH mixture (4/1 v/v).

Table 1. Room temperature photophysical, nonlinear and chiroptical data for the two **Λ-Er** and **Δ-Er** complexes in MeOH.

	Λ-Er	**Δ-Er**
λ_{max} (nm)	455	455
ε (L.mol^{-1}.cm^{-1})	102000	117000
λ_{em} (nm)	1520	1519
τ (ns)	212	213
g_{abs}(233)	-0.01509	0.01408
g_{abs}(452)	-0.00016	0.00016
g_{lum}(1519)[a]	-0.66	0.66

a: with an EBW of 3.2 nm.

Upon excitation in the ILCT transition of the complexes **Δ-Er** and **Λ-Er** the characteristic erbium centered transition at 1520 nm is observed that can be assigned to the $^4I_{13/2} \rightarrow {}^4I_{15/2}$ transition

(Fig. 3, bottom, Figure S14-15). The room temperature spectrum is quite broad, displaying 7-8 main bands. It is worth noting that in D_3 symmetry the $^4I_{15/2}$ ground state (and the $^4I_{13/2}$ excited state) is split in 8 (and 7) different m_J sub-levels following the crystal field splitting theory.[22] Consequently, the maximum number of potential transitions is then 8 × 7 = 56. Upon cooling down to 77 K in an organic glass most of the $m_{J'}$ excited sub-levels are depopulated resulting in a surprisingly well-resolved spectrum. Nevertheless, this spectrum still contains several overlapping transitions making a comprehensive crystal field splitting assignment unfeasible. The luminescence lifetime has been measured and is nicely fitted by a mono-exponential decay (Figure S16) yielding a value of τ = 212 ns for **Λ-Er** and 213 ns for **Δ-Er**, respectively.[17, 23]

ECD and CPL measurements have also been performed for both complexes in methanol. A clear intense ECD signature is observed for the UV-transition around 233 nm assigned to the π–π* transition of the naphtyl sub-units close to the chirality center (Figure S17 and Table 1). Interestingly, the charge transfer band delocalized on the complete conjugated skeleton also presents an ECD signature centered at 450 nm but with a smaller intensity.

In contrast, no sufficiently strong luminescence and consequently no CPL signal could be measured in the range of the $^4I_{13/2} \rightarrow {}^4I_{15/2}$ transition. This was solved by using deuterated methanol as solvent resulting in a significant enhancement of the luminescence due to the reduction of non-radiative vibronic quenching.[24] It is worth mentioning that replacing CH_3OH also suppresses reabsorption in the 1450–1650 nm range due to the presence of O-H and C-H overtones.[22] Hence, the luminescence increases, enabling the acquisition of NIR-CPL spectra with a very good S/N for the most intense band observed at 1519 nm (Fig. 4 bottom). Likewise, the absorption spectrum of **Δ-Er** could be acquired in deuterated methanol (Fig. 4 top), despite the very low absorption coefficient of erbium.

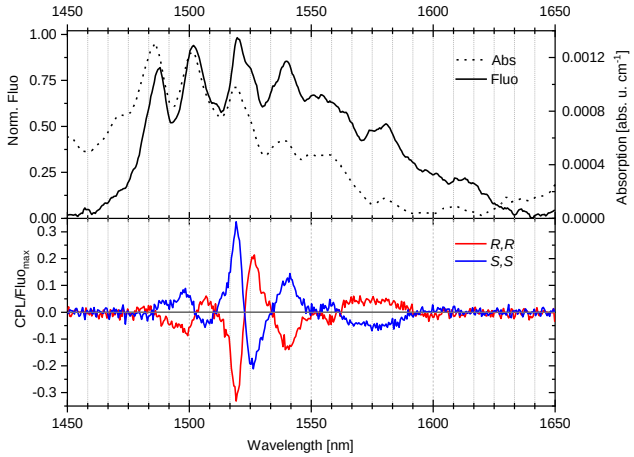

Fig. 4. Top: Room temperature NIR absorption (dashed line) and fluorescence (solid line) spectra of solutions of **Δ-Er** in CD_3OD ($c = 5.0\ 10^{-4}$ M for absorption and $c = 3.4\ 10^{-4}$ M for fluorescence). Bottom: NIR-CPL (CD_3OD, $c = 3.4\ 10^{-4}$ M) of **Δ-Er** (blue) and **Λ-Er** (red), recorded at an EBW of 3.2 nm.

In order to determine the CPL dissymmetry factor g_{lum} defined according to eq. (1), where I_L and I_R stand for the intensity of left and right circularly polarized components of the emission, we envisaged to collect the CPL spectra featuring the highest possible resolution.

$$g_{lum} = \frac{2|I_L - I_R|}{(I_L + I_R)} \quad (1)$$

To achieve this, we experimented with various emission slit aperture settings, ranging from 0.5 to 1.5 and 3 mm, which corresponds to an EBW of 3.2, 10, and 20 nm, respectively (Fig. 5).[‡] To facilitate comparison across these different settings, the CPL spectra were divided by the maximum value of the corresponding emission at each EBW.

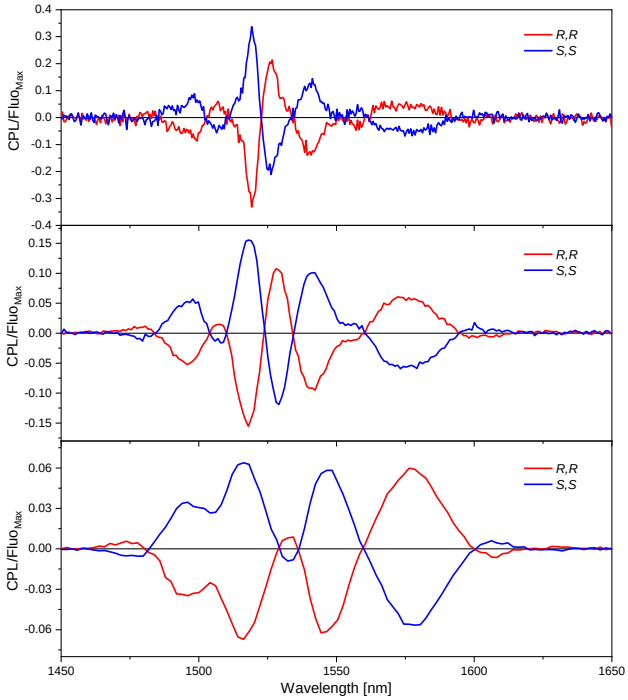

Fig. 5. Room temperature NIR-CPL of a concentrated CD_3OD solution of **Δ-Er** (blue) and **Λ-Er** (red) measured with an EBW of 3.2 nm (top), 10 nm (middle) and 20 nm (bottom).

Naturally, reducing the slit aperture increased the spectral resolution but it simultaneously reduced the signal intensity, resulting in a lower S/N. This is particularly evident when examining the NIR-emission spectra recorded alongside the CPL spectra (Figure S17). Expanding the slit aperture by a factor of 6 (increasing EBW from 3.2 to 20 nm) led to a nearly 10-fold increase in the signal, providing an excellent S/N ratio but causing a substantial loss of resolution. For the CPL spectra, the influence of the EBW is even more pronounced (Fig. 6, top).

While the spectra obtained with a EBW of 3.2 and 10 nm are almost identical, the spectrum with a 20 nm EBW exhibits marked differences. The minor band at 1507 nm (band **C**) is completely masked by the surrounding broad bands (bands **B** and **D**). More importantly, one of the main bands centered at 1527 nm (band **E**) also disappears in the low-resolution spectra. In addition, the positions of the CPL band maxima (or minima) undergo significant shifts with varying the EBW.

Fig. 6. (Top) Merged CPL spectra for **Δ-Er** and **Λ-Er** measured at different experimental bandwidth. (Bottom) Resulting curves of the emission dissymmetry factor g_{lum} over the emission ranges.

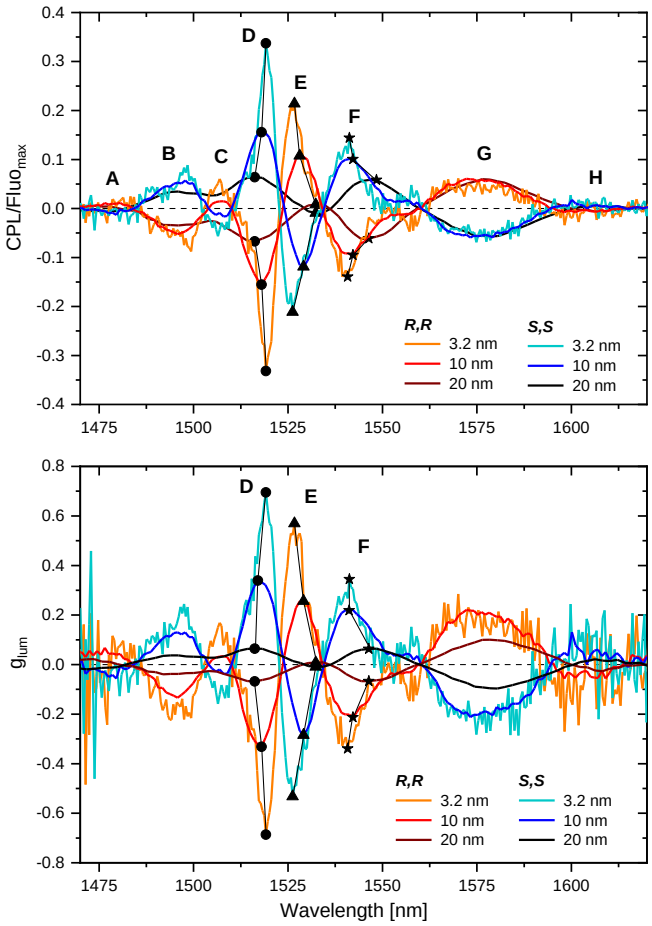

As an example, Fig. 6 illustrates a red-shift of bands **E** and **F** with wider slits, whereas band **D** exhibits a slight blue-shift. These modifications in experimental conditions also have a very strong influence on the g_{lum} determination. To highlight this effect, we measured the dissymmetry factors across the complete emission range at different spectral resolution (Fig. 6, bottom). At room temperature, the maximum g_{lum} value, obtained at the lowest EBW (3.2 nm) is 0.66 at 1519 nm (band **D**) for **Δ-Er** (-0.66 for the other enantiomer). This value is actually the highest compared to already published Er(III) complexes.[4] It is crucial to note that opening the slits results in a significant decrease of this value to 0.34 (1517 nm, EBW = 10 nm) and down to 0.06 (1516 nm, EBW = 20 nm). This effect is likewise significant for band **E** with a decrease of g_{lum} from 0.57 to 0.11 and eventually to -0.01 as the EBW increases, here additionally inducing a change of sign. At this point, it is important to keep in mind that a CPL spectrum (as well as an ECD spectrum) represents the difference between two luminescence spectra giving rise to signals with either positive or negative signs. When operating at low resolution (e.g. high EBW), the overlap of two signals contributes to the final CPL signal whose intensity determines the g_{lum} dissymmetry factors. It is worth noting that Zinna and Di Bari have already warned about the effect of measurement resolution on the accuracy of the dissymmetry factor.[25] Therefore, it is crucial to exercise great care in the recording conditions of the CPL and the corresponding emission spectra to obtain the most accurate g_{lum} possible.

Due to the finite dimension of the slits and the pixels of spectrometers, the light intensity measured at a given wavelength is actually the sum of all the wavelengths collected in the geometrical window created by the system. Mathematically, the recorded spectra are the convolution product of the input spectrum with the impulse response of the apparatus. For monochromators, the impulse response can be modelled by a triangle function proportional to the geometrical slit widths multiplied by the grating dispersion. The width of this function corresponds to the EBW of the spectrometer. Therefore, the spectral distortion coming from the EBW is the convolution of the ideal input spectra with a triangle function, which can be computed with standard software.

In Figure 7, we have computed the effect of the EBW on typical input emission and CPL spectra (using an arbitrary fixed $g_{lum} = \pm 2$) that are composed of two Gaussian bands with the following intrinsic characteristics: (i) equal height, (ii) equal full width at half maximum (Δλ), (iii) various distances between the two peaks ranging from 5Δλ (well-resolved input spectrum, Fig. 7a) down to 1Δλ (poorly resolved input spectrum, Fig. 7d). In the same way, the impact of the instrument resolution on the spectrum has been investigated by modulating the EBW from 0.2Δλ up to 6Δλ.

The upper panels in Fig. 7a-d depict the influence of the EBW on the emission spectra, i.e. two bands of same sign. As expected, increasing of the EBW results in: (i) a progressive broadening of the bands, (ii) the baseline intensity between the peaks deviating from zero and (iii) the two peaks gradually overlapping and eventually merging, leading to a total loss of resolution. This is precisely what we observe in the experimental Er(III) luminescence spectra (Figure S18). It is important to emphasis that the positions of the emission bands remain unaffected by the EBW meaning that as soon as peaks are observable, their positions cannot be misinterpreted whatever the device resolution.

In contrast, to the best of our knowledge, the impact of the EBW on CPL spectra has not been previously described and presents added complexity, primarily due to the potential contribution of bands with opposite signs. First, if the CPL spectrum is composed of two bands of the same sign and same intensity, the effect on the CPL is the same as described above for the emission. Therefore, the g_{lum} values are constant whatever the EBW. All other cases are much more complicate because the convolution will have different impact on the emission and CPL spectra resulting in recorded g_{lum} depending on the experimental conditions.

In the following, we focus on the situation where the two CPL bands have opposite sign but equal intensity. The outcome of the calculation under these conditions are illustrated by the middle panels in Fig. 7. It reveals that, as for the emission spectra, the CPL bands broaden when EBW increases. Concerning the baseline, it always intersects the wavelength axis (zero-axis) whatever the EBW.

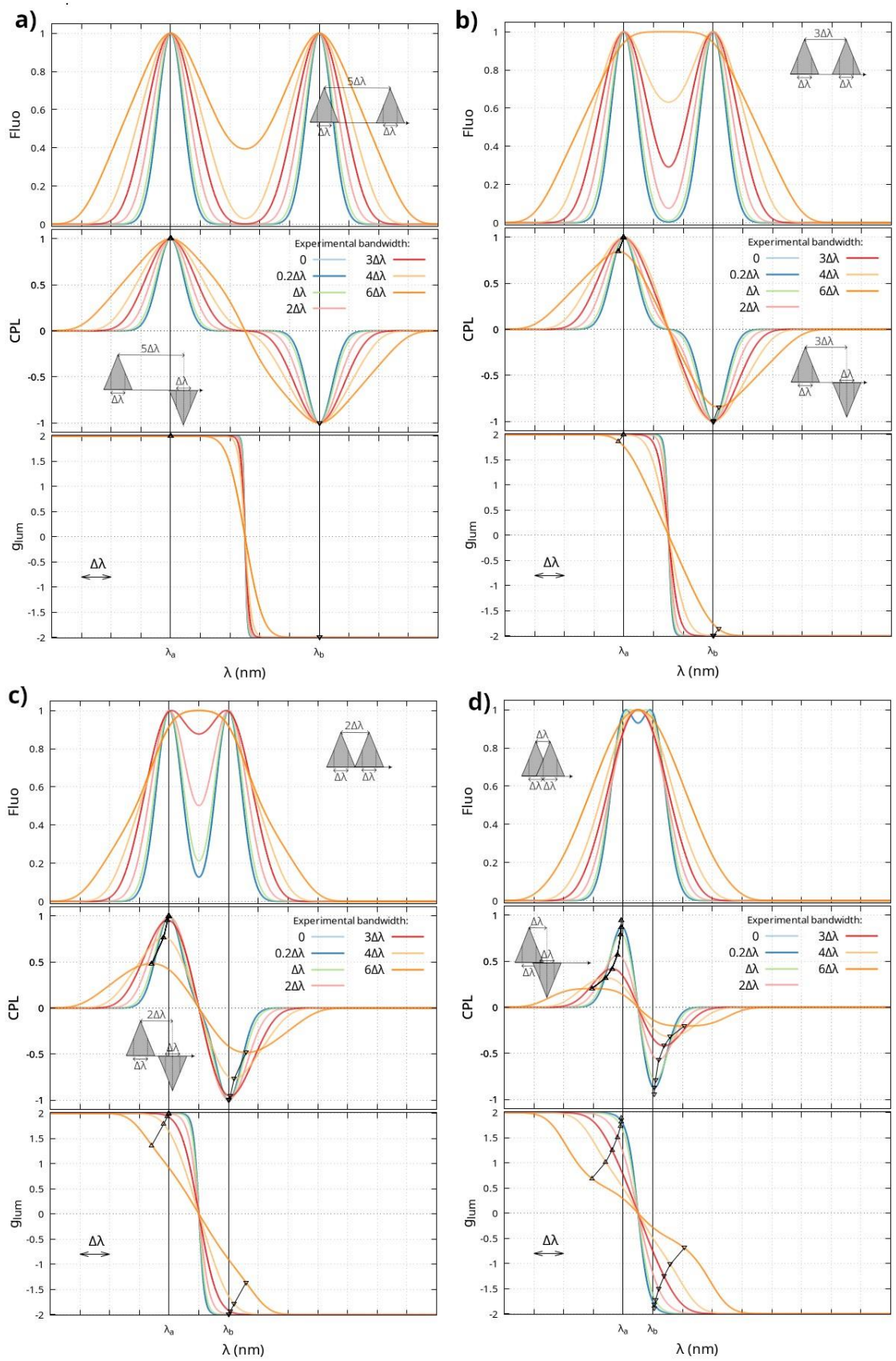

Fig. 7. Convolution of two Gaussian bands (FWHM=Δλ) with triangle functions at various bandwidths from 0 to 6Δλ. Upper panels: evolution of the fluorescence spectra composed of two bands of same sign. Middle panels: evolution of the CPL spectra composed of two bands of opposite sign. Bottom panel: evolution of the g_{lum} values calculated as the ratio between the CPL and the fluorescence. Dotted black curves: evolution of the extrema of CPL intensity and g_{lum}. The distance between the two peaks is a) 5 Δλ, b) 3 Δλ, c) 2 Δλ, d) Δλ.

Nevertheless, the slope of the CPL curve at the zero-axis intersection point depends on both the intrinsic resolution of the spectrum and the EBW. For intrinsically well resolved spectra, the baseline intensity between the CPL bands remains at zero, resulting in an horizontal slope as long as the EBW does not induce any overlap between the peaks (Fig. 7a,b). However, when EBW increases and the CPL bands gradually overlap, this slope deviates from zero. At low intrinsic resolution, the overlap between the CPL bands gives rise to a non-zero slope at the zero-axis crossing point regardless of the EBW (Fig. 7c,d). In these cases, the CPL curve's slope decreases with increasing EBW. This is accompanied by a shift in the CPL peak positions as indicated by the dotted black curve showing that the spectral gap between the two bands' extrema increases with the EBW, while it stays constant for the emission spectra. The apparent transitions observed in the CPL spectra at λ_{peak} do not match anymore the intrinsic transitions visible in the luminescence spectra. This phenomenon is accompanied by a change in intensities resulting in a $g_{lum}(\lambda)$ which is no more constant over the transitions as shown in the Fig. 7b,c,d lower panels. As a consequence of the mixing of two CPL opposite contributions, the g_{lum} value decreases together with the resolution.

We have also explored additional scenario, where the two transitions have CPL bands of different intensities (in the ratio 1/5) and with the same or opposite signs. The simulated luminescence and CPL spectra as a function of the EBW and the evolution of the g_{lum} factor are detailed in the Supporting Information (Figures S19-S20). The evolution is qualitatively the same: increasing EBW induces a decrease of the g_{lum} and a peak displacement. However, the intensity of this shift is less pronounced. For a better rationalization of these observations, it appears relevant to compare the resolution factors R of the recorded spectra as function of the EBW. The resolution factor is the distance between the two transitions normalized by their widths:

$$R=\frac{\lambda_b-\lambda_a}{\Delta\lambda_a+\Delta\lambda_b}$$

where λ_a (λ_b) and $\Delta\lambda_a$ ($\Delta\lambda_b$) are the wavelength and width of the transitions (a) and (b), respectively. High resolution factors correspond to well resolved transitions whose relative distances are higher than their widths.

We note R_{in} the intrinsic resolution factor of the emitted light (i.e. recorded with an ideal (EBW = 0) instrument). As instruments have non null EBW, recorded signals have wider widths than the intrinsic one's (the higher EBW the higher the recorded width). We have visualized in Fig. 8 the evolution of the calculated resolution factors of the recorded spectra as a function of the EBW for five different input signals characterized by two fluorescence lines with resolution factor R_{in} and opposite CPL lines with same intensities. The figure displays the output resolution factor calculated for the fluorescence (continuous lines) and CPL spectra (dotted lines), $R_{out\text{-}Fluo}$ and $R_{out\text{-}CPL}$, respectively. As before, the measured signals are the convolution of the input one's with a triangle function of width EBW. As expected, the higher the EBW, the lower the resolution of the recorded emission spectra $R_{out\text{-}Fluo}$. The resolution factor of the CPL spectra perfectly matches the fluorescence's one for high R_{in} and low EBW. For high EBW, $R_{out\text{-}CPL}$ becomes higher than $R_{out\text{-}fluo}$ and the lower R_{in} the higher $R_{out\text{-}CPL}$. For the poorly resolved $R_{in} = 1$ spectra, $R_{out\text{-}CPL}$ is even higher than one. This behavior is extremely annoying because it means that the observation of well-separated peaks in the CPL spectra (high $R_{out\text{-}CPL}$) does not guarantee the trueness of the spectra. This is owed to the circumstance that the CPL peak displacement is higher than the spectral broadening (see Fig. 7c and d).

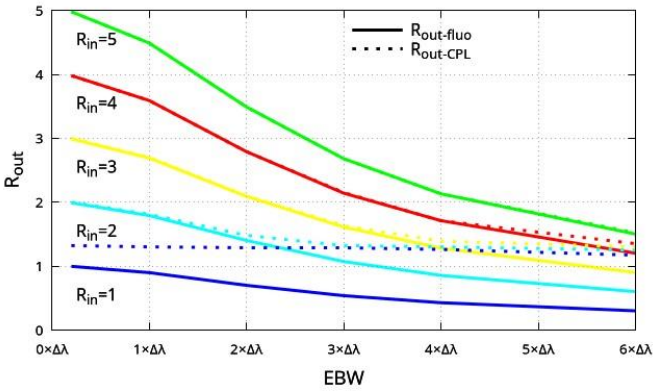

Fig. 8. Evolution of the resolution factors $R_{out\text{-}Fluo}$ (continuous lines) and $R_{out\text{-}CPL}$ (dashed lines) as a function of the EBW and for several initial intrinsic conditions R_{in} for two bands of opposite signs overlapping.

Practically speaking, the quantitative analysis of CPL signals (determination of g_{lum} values) is based on finding the position of the transitions and their intensities as defined in eq.(1). For this we have computed the peak shifts and g_{lum} as a function of EBW. Fig. 9 (continuous curves) shows the influence of EBW on the λ_{peak} shift defined as $\lambda_{peak} - \lambda_{in}$ where λ_{in} is the intrinsic position of the transition (EBW = 0). For well resolved signals ($R_{in}>4$), there are no apparent shifts in the recorded spectra whatever the EBW and $\lambda_{peak} - \lambda_{in} = 0$ (red and green curves have zero value). However, for intrinsically less resolved input signals (low R_{in}), the higher the EBW, the higher the peak shift. Fig. 9 (dashed curves) also makes clear that the g_{lum} decreases with EBW especially when the considered transitions are poorly resolved (low R_{in}).

These findings can lead to bad quantifications and may explain some discrepancies reported in literature. Contrary to standard spectroscopy, an apparent increase in the resolution of the spectrum does not guarantee a valid measurement. One condition accounting for a reliable exploitation of the signal is the CPL curve slope at the zero-axis crossing point to be zero, attesting for the non-overlapping of transitions. In case of a residual overlap, great care should be taken. Indeed, the measured peaks may not reflect the individual CPL molecular transitions in neither position nor intensity. Worse, certain peaks can even be hidden and/or change signs. To a certain extent, this can be improved by optimizing the spectrometer resolution through the decreases of the slit width until the recorded spectra, both emission and CPL, remain unchanged.

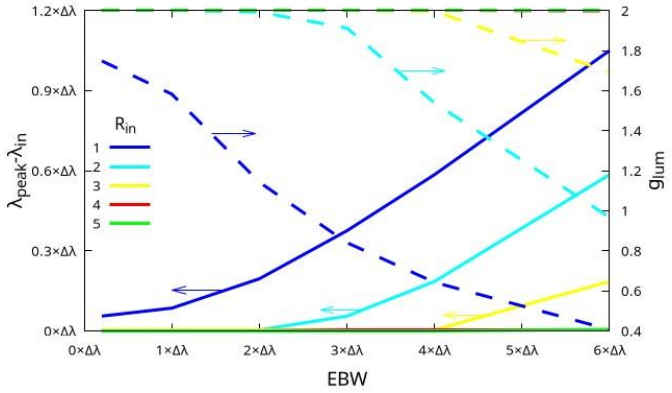

Fig. 9. Evolution of the CPL peak shift $\lambda_{peak} - \lambda_{in}$ (continuous, left axis) and of the g_{lum} at λ_{peak} (dashed, right axis) as a function of the EBW and for several initial intrinsic conditions R_{in} for two bands of opposite signs and same intensities.

Conclusions

We report in this article the synthesis and the complete chemical, photophysical and chiroptical characterization of a pair of Er(III) enantiomers featuring a controlled Δ- and Λ-helicity. This complexes present NIR-CPL signature with a very high g_{lum} value of 0.66 for the band at 1519 nm at room temperature. Due to the excessive number of possible transitions at room temperature (theo. 56) it is impossible to assign this band to a well-defined crystal field splitting transition and it most likely results from the overlapping of many contributions. To refine the spectral analysis, we explore the effect of reduction of the EBW by monitoring the slit aperture of our CPL apparatus. From a practical point of view, from our simulations, we were able to extract good practices for the measurement of CPL spectra. Counterintuitively, CPL spectra with well resolved peak provide no guarantee that the CPL lines are not overlapping. A better signature of the low resolution is the slope of the CPL at the crossing point: if non-zero it means that two neighbor lines overlap. Moreover, the loss of resolution for two CPL peaks of opposite signs induces two main drawbacks: (i) the position of the CPL peak does not reflect necessary the *true* position of the CPL contributions and (ii) the measured values of g_{lum} are underestimated. To conclude, when reporting CPL spectra the knowledge of the experimental resolution is of prime importance in order to estimate the trueness of the results.

Author Contributions

OM, FR, BLG and SG designed and supervised the study. / AS synthetized and characterized the complexes. / FP and OC solved the XRD structures. / AS, OM and FR performed the non-polarized spectroscopy. / YG measured the NIR emission decays. / AS, BB, LG, ABL and SG performed all the chiroptical measurements. / MG and BLG carried out the multireference wavefunction simulations. / SG and LG designed and performed the numerical simulations. All the authors discussed and contributed to the manuscript preparation. / All authors have given approval to the final version of the manuscript.

Conflicts of interest

There are no conflicts to declare.

Acknowledgements

Authors acknowledge support from Agence Nationale de la Recherche (SMMCPL ANR-19-CE29-0012-02).

Notes and references

‡ EBW is the intrinsic apparatus resolution and depends on the grating and the monochromator output focal length. In the present case with a CS260 Oriel/Newport monochromator equipped with a Newport 74067 grating, EBW = 6.4 nm /mm.

References

1. C. L. Maupin, D. Parker, J. A. G. Williams and J. P. Riehl, Circularly Polarized Luminescence from Chiral Octadentate Complexes of Yb(III) in the Near-Infrared, *J. Am. Chem. Soc.* 1998, **120**, 10563-10564.
2. L. Di Bari, G. Pintacuda and P. Salvadori, Stereochemistry and Near-Infrared Circular Dichroism of a Chiral Yb Complex, *J. Am. Chem. Soc.*, 2000, **122**, 5557-5562.
3. C. L. Maupin, R. S. Dickins, L. G. Govenlock, C. E. Mathieu, D. Parker, J. A. G. Williams and J. P. Riehl, The Measurement of Circular Polarization in the Near-IR Luminescence from Chiral Complexes of Yb(III) and Nd(III), *J. Phys. Chem. A*, 2000, **104**, 6709-6717.
4. O. G. Willis, F. Zinna and L. Di Bari, NIR-Circularly Polarized Luminescence from Chiral Complexes of Lanthanides and d-Metals, *Angew. Chem. Int. Ed.*, 2023, **n/a**, e202302358.
5. F. Zinna, L. Arrico and L. Di Bari, Near-infrared circularly polarized luminescence from chiral Yb(iii)-diketonates, *Chem Commun*, 2019, **55**, 6607-6609.
6. O. G. Willis, F. Zinna, G. Pescitelli, C. Micheletti and L. Di Bari, Remarkable near-infrared chiroptical properties of chiral Yb, Tm and Er complexes, *Dalton Trans.*, 2022, **51**, 518-523.
7. E. Kreidt, L. Arrico, F. Zinna, L. Di Bari and M. Seitz, Circularly Polarised Luminescence in Enantiopure Samarium and Europium Cryptates, *Chem. Eur. J.*, 2018, **24**, 13556-13564.
8. B.-A. N. Willis, D. Schnable, N. D. Schley and G. Ung, Spinolate Lanthanide Complexes for High Circularly Polarized Luminescence Metrics in the Visible and Near-Infrared, *J. Am. Chem. Soc.*, 2022, **144**, 22421-22425.
9. E. Cavalli, C. Nardon, O. G. Willis, F. Zinna, L. Di Bari, S. Mizzoni, S. Ruggieri, S. C. Gaglio, M. Perduca, C. Zaccone, A. Romeo and F. Piccinelli, Near Infared Circularly Polarized Luminescence From Water Stable Organic Nanoparticles Containing a Chiral Yb(III) Complex, *Chem. Eur. J.*, 2022, **28**, e202200574.
10. S. Mizzoni, S. Ruggieri, A. Sickinger, F. Riobé, L. Guy, M. Roux, G. Micouin, A. Banyasz, O. Maury, B. Baguenard, A. Bensalah-Ledoux, S. Guy, A. Grichine, X.-N. Nguyen, A. Cimarelli, M. Sanadar, A. Melchior and F. Piccinelli, Circularly polarized activity from two photon excitable europium and samarium chiral bioprobes, *J. Mater. Chem. C*, 2023, **11**, 4188-4202.
11. B. Lefeuvre, C. A. Mattei, J. F. Gonzalez, F. Gendron, V. Dorcet, F. Riobe, C. Lalli, B. Le Guennic, O. Cador, O. Maury,

S. Guy, A. Bensalah-Ledoux, B. Baguenard and F. Pointillart, Solid-State Near-Infrared Circularly Polarized Luminescence from Chiral Yb(III) -Single-Molecule Magnet, *Chem. Eur. J.*, 2021, **27**, 7362-7366.

12. C. A. Mattei, V. Montigaud, B. Lefeuvre, V. Dorcet, G. Argouarch, O. Cador, B. Le Guennic, O. Maury, C. Lalli, Y. Guyot, S. Guy, C. Gindre, A. Bensalah-Ledoux, F. Riobe, B. Baguenard and F. Pointillart, Circularly polarized luminescence in the one-dimensional assembly of binaphtyl-based Yb(iii) single-molecule magnets, *J Mater Chem C*, 2023, **11**, 7299-7310.
13. K. Dhbaibi, M. Grasser, H. Douib, V. Dorcet, O. Cador, N. Vanthuyne, F. Riobe, O. Maury, S. Guy, A. Bensalah-Ledoux, B. Baguenard, G. Rikken, C. Train, B. Le Guennic, M. Atzori, F. Pointillart and J. Crassous, Multifunctional Helicene-Based Ytterbium Coordination Polymer Displaying Circularly Polarized Luminescence, Slow Magnetic Relaxation and Room Temperature Magneto-Chiral Dichroism, *Angew. Chem. Int. Ed.*, 2023, **62**, e202215558.
14. F. Gendron, S. Di Pietro, L. Abad Galán, F. Riobé, V. Placide, L. Guy, F. Zinna, L. Di Bari, A. Bensalah-Ledoux, Y. Guyot, G. Pilet, F. Pointillart, B. Baguenard, S. Guy, O. Cador, O. Maury and B. Le Guennic, Luminescence, chiroptical, magnetic and ab initio crystal-field characterizations of an enantiopure helicoidal Yb(iii) complex, *Inorg. Chem. Front.*, 2021, **8**, 914-926.
15. N. F. M. Mukthar, N. D. Schley and G. Ung, Strong Circularly Polarized Luminescence at 1550 nm from Enantiopure Molecular Erbium Complexes, *J. Am. Chem. Soc.*, 2022, **144**, 6148-6153.
16. J. A. Adewuyi, N. D. Schley and G. Ung, Vanol-Supported Lanthanide Complexes for Strong Circularly Polarized Luminescence at 1550 nm, *Chem. Eur. J.*, 2023, e202300800.
17. O. G. Willis, A. Pucci, E. Cavalli, F. Zinna and L. Di Bari, Intense 1400–1600 nm circularly polarised luminescence from homo- and heteroleptic chiral erbium complexes, *J. Mater. Chem. C*, 2023, DOI: 10.1039/d3tc00034f.
18. O. G. Willis, F. Petri, G. Pescitelli, A. Pucci, E. Cavalli, A. Mandoli, F. Zinna and L. Di Bari, Efficient 1400–1600 nm Circularly Polarized Luminescence from a Tuned Chiral Erbium Complex, *Angew. Chem. Int. Ed.*, 2022, **61**, e202208326.
19. J. P. Leonard, P. Jensen, T. McCabe, J. E. O'Brien, R. D. Peacock, P. E. Kruger and T. Gunnlaugsson, Self-Assembly of Chiral Luminescent Lanthanide Coordination Bundles, *J. Am. Chem. Soc.*, 2007, **129**, 10986-10987.
20. K. Sénéchal-David, A. Hemeryck, N. Tancrez, L. Toupet, J. A. G. Williams, I. Ledoux, J. Zyss, A. Boucekkine, J.-P. Guégan, H. Le Bozec and O. Maury, Synthesis, Structural Studies, Theoretical Calculations, and Linear and Nonlinear Optical Properties of Terpyridyl Lanthanide Complexes: New Evidence for the Contribution of f Electrons to the NLO Activity, *J. Am. Chem. Soc.*, 2006, **128**, 12243-12255.
21. A. Picot, F. Malvolti, B. Le Guennic, P. L. Baldeck, J. A. G. Williams, C. Andraud and O. Maury, Two-Photon Antenna Effect Induced in Octupolar Europium Complexes, *Inorg. Chem.*, 2007, **46**, 2659-2665.
22. J.-C. G. Bünzli and S. V. Eliseeva, in *Lanthanide Luminescence: Photophysical, Analytical and Biological Aspects*, eds. P. Hänninen and H. Härmä, Springer Berlin Heidelberg, Berlin, Heidelberg, 2011, DOI: 10.1007/4243_2010_3, pp. 1-45.
23. S. W. Magennis, A. J. Ferguson, T. Bryden, T. S. Jones, A. Beeby and I. D. W. Samuel, Time-dependence of erbium(III) tris(8-hydroxyquinolate) near-infrared photoluminescence: implications for organic light-emitting diode efficiency, *Synth. Met.*, 2003, **138**, 463-469.
24. E. Kreidt, C. Kruck and M. Seitz, in *Including Actinides*, 2018, DOI: 10.1016/bs.hpcre.2018.04.001, pp. 35-79.
25. F. Zinna, L. Di Bari, Lanthanide Circularly Polarized Luminescence: Bases and Applications, *Chirality*, 2015, **27**, 1-13.